The Pennsylvania State University
College of Earth and Mineral Sciences
Department of Geosciences

Environmental Niche Model for Iron-Oxidizing Bacteria in Pennsylvania Acid Mine Drainage

A Senior Thesis in Geobiology

by

Courtney A. Kolesar

Submitted in Partial Fulfillment
of the Requirements
for the Degree of

Bachelor of Science

May, 2012

We approve this thesis:

[redacted]

1 May 2012

Jennifer Macalady Professor of Geosciences — Date

[redacted]

2 May 2012

Mark Patzkowsky, Associate Professor of Geosciences
Associate Head of the Undergraduate Program — Date

Contents

Abstract

Ecological niche models are an essential tool in understanding the relationship between geochemical parameters and the residing microbiology within an environmental system. This study examined three Pennsylvania acid mine drainage (AMD) systems (Sulphur Run, Windber, and Upper Red Eyes) to explore correlations between the stream's chemical properties and iron-oxidizing bacteria. Fluorescent in situ hybridization (FISH) and DNA extraction and sequencing were used to observe the abundance and distribution of iron-oxidizing bacteria at multiple locations downstream from each AMD emergence. *Gallionella, Ferrovum,* and *Acidithiobacillus* were the dominant taxa overall, and each exhibited a favorable location from the emergence downstream in each AMD system. The relative abundance values and distribution results showed generally weak correlations with all geochemical measurements including pH. However, when the results were extrapolated onto and compared to a previously developed pH/[Fe^{2+}] AMD niche model, each taxa clearly clustered within specific pH/[Fe^{2+}] niches. *Gallionella* abundance values from this study increased the [Fe^{2+}] range from 550 mg/L-400 mg/L to 550mg/L-75mg/L. *Ferrovum* and *Acidithobacillus* abundances are greatest in pH 2.5 -3/[Fe^{2+}] 200mg/L - 350 mg/L and pH 2-3 / [Fe^{2+}] <270 mg/L respectively. This study defined a multivariate geochemical niche model which can be used to accurately predict the microbial community composition and structure. Such a model can be useful for environmental engineers attempting to remediate AMD systems.

1.0 Introduction

Acid mine drainage (AMD) is an important global environmental hazard that drastically alters the biogeochemistry of streams emerging from mine portals or tailings (McKnight and Feder, 1984). It is believed that the formation of AMD is accelerated by iron-oxidizing bacteria (Gonzalez-Toril et al., 2011; Nancucheo and Johnson, 2011; Weber et al., 2010). These microbes enhance the rate of sulfide dissolution by generating more ferrous iron than what would occur chemically. In this way, microbial activity may be responsible for the bulk of AMD generated. However, a recently proposed bioremediation method utilizes the microbial iron-oxidation to its advantage. To implement such a method, the geochemical conditions favorable for the each type of iron-oxidizing bacteria must be thoroughly understood.

It is hypothesized that the geochemistry of an environmental system determines the distribution and abundance of the microbial community. This study aims to test that hypothesis and shed light on the geochemical and biological relationship dynamics of acid mine drainage. Although geomicrobiological characteristics of AMD systems have been extensively characterized (Druschel et al., 2004; Gonzalez-Toril et al., 2011; He et al., 2007; Heinzel et al., 2009; Lear et al., 2009), these dynamics remain largely unknown. The underlying objectives are to 1) describe the microbial community structure and the quantification of microbial diversity associated with AMD 2) investigate the physical and chemical parameters that define the distribution and diversity of iron-oxidizing bacteria within AMD and 3) extrapolate the bacterial abundance values onto a preexisting pH/[Fe^{2+}] niche model (Jones et al., In preparation)to test the previous hypothesis. To achieve this, the microbial-geochemical interplay of three distinct AMD sites (Upper Red Eyes, Windber, and Sulfur Run) is examined using DNA extraction and sequence cloning coupled with florescent *in situ* hybridization (FISH). These systems are

geochemically distinct from one another, allowing a comparison between geochemical parameters and the resulting microbiology. Conveniently, the AMD systems are all within 15 miles from the AMD system, Lower Red Eyes, studied by (Jones et al., In preparation).

The global occurrence and ecological destructiveness of AMD demands attention and remediation. The relatively simplistic geochemical framework renders AMD systems valuable models for biogeochemical feedbacks between the microbiology and the environment necessary for remediation progress. This study will not only provide insight essential for understanding the dynamics between the physical and biological characteristics in AMD for niche dynamic examination but will also enhance important bioremediation efforts. Accurate AMD niche models will allow researchers to predict the inherent microbial community structure and composition by simply measuring the geochemistry within the stream, decreasing remediation development time and eliminating the need for in depth microbial examination.

2.0 Background

2.1 AMD microbiology and niche models

The term “niche” is defined as a combination of resources and environmental conditions that allow survival and reproduction (Meyer and Leveau, 2012). More specifically, it is a concept developed to describe all physical and chemical parameters which determine a certain ecological role unique to any given organism. Studies aim to accurately and fully describe organism niches in order to understand the relative relationships within biogeography. Unfortunately, the inherent complexity of niche partitioning is largely unknown and has been a focus for debate for some time (de Wit and Bouvier, 2006)**.** To address this problem, researchers are focusing on less complex communities such as the microbial communities in acid mine drainage (AMD) systems.

In general, the overall diversity of bacteria within AMD systems is low and the dominant microbial composition changes with distance downstream (Baker and Banfield, 2003). The common iron oxidizing bacteria found in AMD are *Acidithiobacillus ferroxidans, Leptospirillum ferroxidans, Ferrimicrobium acidiphilium, Ferrovum,* and novel acidophilic Gallionella-like bacteria (Druschel et al., 2004; Gonzalez-Toril et al., 2011; He et al., 2007; Heinzel et al., 2009; Lear et al., 2009). Many studies investigate bacterial community structure and subsequently compare the results to each geochemical parameter individually. Bacterial distribution and abundance are most attributed to pH (Brown et al., 2011; Lear et al., 2009), although other geochemical conditions (Fe(II), dissolved oxygen, temperature) may play an important role in bacterial distribution (Gonzalez-Toril et al., 2011). However, a convincing correlation between the microbial compositions and distributions and the geochemical parameters has yet to be discovered.

A previous study used multivariate analysis to elucidate the most influential geochemical factors determining the abundance and distribution of iron-oxidizing bacteria in the Lower Red Eyes AMD system (Jones et al., In preparation). Results showed that pH and ferrous iron best described the iron-oxidizing bacterial structure and when plotted against each other, taxa clusters emerge within specific pH/ $[Fe^{2+}]$ ranges. The current study uses an expanded data set to test the Jones et al. niche model hypothesis and improve its accuracy.

2.2 AMD Biogeochemistry

Although AMD is a global phenomenon, over one-third of the world's streams impacted worldwide are located in Pennsylvania (Engineers, 1969). The Corp of Engineers reports that a century of coal mining has caused AMD to contaminate over 2,500 miles of PA streams. Coal mining exposes pyrite to air and water (Templeton, 2011). When exposed, sulfide ores dissolve

(or oxidize) which ultimately increases the stream acidity and precipitates high concentrations of metals (Fe, Al, Mn, Cu, Zn, Cd, As, Pb, Co, and Ni) that are then transported to rivers and water reservoirs. Equations 1- 4 show the generl abiotic and biotic reactions that take place.

Eq. 1 $2FeS_2\ (s) + 7O_2 + 2H_2O \rightarrow 2Fe^{2+} + 4SO4^{2-} + 4H^+$

Eq. 2 $2Fe^{2+} + ½\ O_2 + 2H^+ \rightarrow 2Fe^{3+} + H_2O$

Eq. 3 $2Fe^{3+} + 6H_2O \rightarrow 2Fe(OH)_3\ (s) + 6H^+$

Eq. 4 $FeS_2 + 14\ Fe^{3+} + 8\ H_2O \rightarrow 15\ FeS^{2+} + 2\ SO_2^{4-} + 16\ H^+$

The end product is acidic (~pH 4-pH 2) waters that can drastically destroy the surrounding ecosystem and pollute reservoir waters (Dsa et al., 2008; Gerhardt et al., 2008).

Equation 1 shows the abiotic reaction of iron sulfide through oxygen exposure yielding ferric iron. The ferric iron is further oxidized to ferrous iron by iron oxidizing bacteria (Eq. 2). Ferrous iron can react with water to form iron hydroxide (Eq. 3) or it can react with iron sulfide in an oxygen independent reaction (Eq. 4). Combined, these abiotic and biotic reactions lower the pH from neutral to a pH of 2-4 depending on the distance downstream. It is important to note that iron oxidizing bacteria have a profound effect on the acid producing rate of an affected stream. Acidophilic iron-oxidizing bacteria can accelerate the rate of pyrite oxidization by several orders of magnitude (Dsa et al., 2008). Therefore, characterizing the microbial community, specifically the iron oxidizing bacteria, is crucial for not only understanding the local geochemical processes, but also for remediation efforts.

2.3 Remediation Efforts

The extensiveness of AMD has led to numerous remediation methods (Mohapatra et al., 2011; Sheoran and Sheoran, 2006). Generally, the remediation methods used are site specific, depending on the character of the abandoned mine, the amount of space affected, and the severity of the damage. Methods used thus far group into two main categories: source control and migration control. Source control includes methods such as flooding and sealing of underground mines, underwater storage of mine tailings, land based storage in sealed waste heaps, mineral waste blends, total solidification of tailing, application of anionic surfactants, and microencapsulation. These methods are used prior to AMD formation limiting the number of sites that are able to be remediated. Further limitations include weather, effectiveness, and cost.

Migration control methods divided into two categories: abiotic and biotic. Abotic methods further subdivide into active and passive systems. Active abitoic methods include systems such as aeration and lime addition and passive systems include anoxic limestone drains. While the active methods are relatively simple with respect to development, time, and cost, the effectiveness is highly variable and the costs are great. Furthermore, some of the active methods leave behind a bulky sludge producing disposal problems. Passive abiotic migration methods are generally lower in cost than active migration methods, but are not suitable for all AMD systems. When remediated with a passive abiotic migration system, streams with a significant amount of ferric iron or aluminum produce precipitates on the drains gradually decreasing the drain permeability. Biotic migration control methods provide a more effective solution for active AMD remediation. Unlike the abiotic methods, biotic methods are usually more effective and require far less maintenance, however the costs can be twice as much as abiotic methods.

Results from this study will aid in efforts to create a more effective, sustainable, and affordable bioremediation system than the existing remediation techniques. A recently proposed bioremediation method utilizes the microbial iron-oxidation to its advantage, creating conditions in which limestone can neutralize the waters without becoming covered in iron precipitate.

3.0 Methods

3.1 Field Geochemistry

Three AMD sites were analyzed in this study and compared to a previously studied site called Lower Red Eyes (Brown et al., 2011). Upper Red Eyes is the neighboring site to Lower Red Eyes rendering the site a reasonable system for geochemical comparison. Windber and Sulfur Run were chosen to compare to Lower Red Eyes because of the drastically different pH characteristic. Appendix A shows the stream geochemistry measured in the field as previously described (Brown et al., 2011) and the geographic locations of each stream. The dissimilar geochemistry between the four sites enabled the study of the effect that pH and ferrous iron concentration have on the abundance and distribution of iron oxidizing bacteria.

Seven samples were taken from Upper Red Eyes on April 2011 along a flowpath from the emergence (0 feet) to 506 feet downstream. Sample UR 100 was taken at the most uphill emergent source from about 2 feet inside the emergent pool.

Table 1 . Upper Red Eyes sample locations and respective distance downstream from

Site ID	Distance from emergence (ft)
UR100	0
UR84	53
UR83	55
UR82	175
UR80	258
UR70	358
UR60	506

Samples UR84, UR83, UR82, UR80, and UR70 were taken 53 feet, 55 feet, 175 feet, 258 feet, and 358 feet downstream respectively (Table 1).

Three samples were taken from Windber on September of 2011 along a flowpath from the emergent AMD spring (0 feet) to 175 feet downstream. Sample WB50 was taken directly from the emergence at the top of a steep iron-coated hillside.

Table 2 . Windber sample locations and respective distance downstream from the

Site ID	Distance from emergence (ft)
WB50	0
WB30	105
WB20	175

Sample WB30 was 105 feet from the emergence along an “iron slide” close to the same elevation as the bottom of a large coal pile directly adjacent to the slide. Sample WB20 was taken 175 feet from the emergence approximately halfway down the iron hillside and just uphill from where the scoured channels split and diverge (Table 2).

Three samples were taken from Sulphur Run in September of 2011. Sample SR50 was taken directly from the emergence.

Table 3. Sulphur Run sample locations and respective distance downstream from the

Site ID	Distance from emergence (ft)
SR50	0
SR20	204
SR10	228

Sample SR20 was taken 204 feet from the emergence and SR10 was taken 228 feet from the emergence (Table 3).

3.2 Sample Collection and Preservation

Samples were collected at locations where geochemical data had been taken. Bulb tubes (5mL) were used to extract sediment (roughly 3 to 5 grams) from the sediment/water interface. The water and sediment were stored in 5mL centrifuge tube on ice for cell preservation until sample collection was complete. The samples were fixed by the following procedure:

- 1 mL of sample centrifuged at 15000 rpm for 2 minutes at 4°C.
- Samples decanted and resuspended in 500 µl of cold 1xPBS and 500 µl of 98% ethanol fixative and incubated for 2 hours at 4°C.
- Samples centrifuged as previously directed and resuspended to a volume of 1 mL with 1XPBS to additional times.

After the final resuspention, the sample tubes were filled to the original volume (1 ml) using a 98% ethanol fixative. The fixed cells were stored at 4°C. Unfixed cell samples were stored at -20°C.

3.3 FISH

Fluorescence in situ hybridization (FISH) analyses were performed as described by Hugenholtz et al. (2001). Briefly, samples were spotted onto 10-well Teflon-coated slides and, after drying, were dehydrated in 50, 80, and 90% ethanol solutions for 3 minutes each (Simmons, 2010). The hybridization buffer was made by mixing 40µL of 1M TRIS at pH 8.0, 2µL 10% SDS, 360µL of 5M NaCl, formamide (concentration varied with probe), and 898 µL of MQ water into a 2mL tube. Eight µL of hybridization buffer was put onto each well of the dried FISH slide followed by 1µL of each probe fluorescently labeled probe (Table 4). After incubation for 2 hours at 46°C, slides were incubated in wash buffer (20 mM Tris-HCl at pH 7.4, 0.01% SDS,

and NaCl, based on reference 20) for 15 minutes at 48°C. Slides were then rinsed with deionized water and stained with 4,6-diamidino-2-phenylindole (DAPI).

Slides were mounted with Vectashield and viewed with a Nikon Eclipse 80i epifluorescence microscope at 1,000X. A monochrome Photometrics Coolsnap ES2 charge-coupled device (CCD) camera was used to obtain photomicrographs with NIS-Elements AS 3.0 software. Population data were generated by counting DAPI-stained cells per probe combination. The mean and standard deviation for each FISH probe were calculated directly from counts of multiple photomicrographs. At least six photos (each taken from a different location with on one well) were counted from at least two slide wells for each probe. FISH photo examples from WB50 using probe Ferri643 can be found in Appendix B.

DAPI and Eubmix were used to target cells and bacteria respectively. A new probe was developed specifically for the acidophilic *Gallionella*-like 16srRNA sequence observed in preliminary AMD clone sequences results (Jones et al., In preparation). To label the *Gallionella* group, we designed probe Gal177mod using the PROBE_DESIGN function in the ARB package (Ludwig et al., 2004). Notice in Table 4 that competitor probes were made (Gal177comp1miss, and Gal177comp1acidi) to target *Acidithiobacilus* and select *Spirilum*.

Table 4
Oligonucleotide probes used in this study

Probe	*Target group*	*Sequence (5' -> 3')*	*% formamide (%)*	*Label*	*Reference*
EUB228[a]	Most bacteria	GCTGCCTCCCGTAGGAGT	0-50	FITC	Amann (1995)
EUB338-II[a]	Planctomycetales	GCAGCCACCCGTAGGTGT	0-50	FITC	Daims et al. (1999)
EUB338-III[a]	Verrucomicrobiales	GCTGCCACCCGTAGGTGT	20	FITC	Daims et al. (1999)
BET42a	Betaproteobacteria	GCCTTCCCACTTCGTTT	35	CY3	Manz et al. (1992)
FERRI643	Ferrovum	ACAGACTCTAGGTTGCA	35	CY3	Brown et al. (2011)
THIO1	Acidithiobacillus	GCG CTT TCT GGG GTC TGC	35	CY5	Gonzalez-Toril et al. (2003)
GAL177mod	Gallionella	TCCCCCTCAGGGCATA	20	CY3	This study
GAL177comp1miss	Competitor	TCCCCCTCAGGGCGTA	20	None	This study
GAL177comp1acidi	Competitor	TCCCCCTCAGGGCTTA	20	None	This sutdy

[a]Combined in equimolar amounts to make EUBMIX

[b]Combined in equimolar amounts to make Gal177mod

Appropriate formamide stringency was determined by using an Upper Red Eyes samples with known 90% *Gallionella* abundance as a positive control and a cultured sample of *Acidithobaci ferrooxidans* as a negative control. Probes Ferri643, ThioCY5, and Bet42a were used to target Gallionella-like bacteria, *Ferrovum*, *Acidithiobacilus*, and β-proteobacteria respectively.

3.4 DNA Extraction, PCR, Cloning, and Sequencing

Sample WB50 was chosen for DNA extraction and sequencing due to preliminary ambiguities within the β-proteobacteria abundance values. The DNA was obtained using phenolchloroform extraction and cloned (Macalady et al., 2008). Colony PCR products of the correct size were purified using the QIAquick PCR purification kit (Qiagen Inc., Valencia, CA, USA) following the manufacturer's instructions. Full-length sequences for 45 clones from each bacterial library were obtained. Clones were sequenced at the Penn State University

Biotechnology Center using M13r and T7 plasmid specific primers. Sequences were assembled with Phred base calling using CodonCode Aligner v.1.2.4 (CodonCode Corp., Dedham, MA, USA) and manually checked for ambiguities. The nearly full-length gene sequences were compared against sequences in public databases using BLAST (Altschul et al., 1990) and submitted to the online analyses CHIMERA_ CHECK v.2.7 (Cole et al., 2003) and Bellerophon 3 (Huber et al., 2004). Putative chimeras were excluded from subsequent analyses. Non-chimeric sequences were aligned using the NAST aligner (DeSantis et al., 2006), added to an existing alignment containing 4,150,000 nearly full-length bacterial sequences in ARB (Ludwig et al., 2004), Phylogenetic trees were computed using maximum parsimony with 1,000 bootstrap replicates computed using PAUP* 4.0b10 (Swofford, 2000).

4.0 Results

4.1 Sulphur Run Microbial distribution and abundance downstream

FISH results revealed the presence of *Gallionella*, *Ferrovum*, and unknown β-proteobacteria within Sulphur Run which show little variation from site SR50 to site SR20 (~25% for both taxa; Figure 1). Further downstream at site SR10, *Gallionella*, *Ferrovum*, and β-Proteobacteria relative abundances increase to 30.77%, 51.72%, and 70%, however, uncertainty associated with low cell counts (Table 5) suggest the possibility of a lesser relative abundance increase. It is important to note that Ferrovum and *Gallionella* constitute only 70% of the total relative β-proteobacteria abundance. The remaining 30% are unknown taxa.

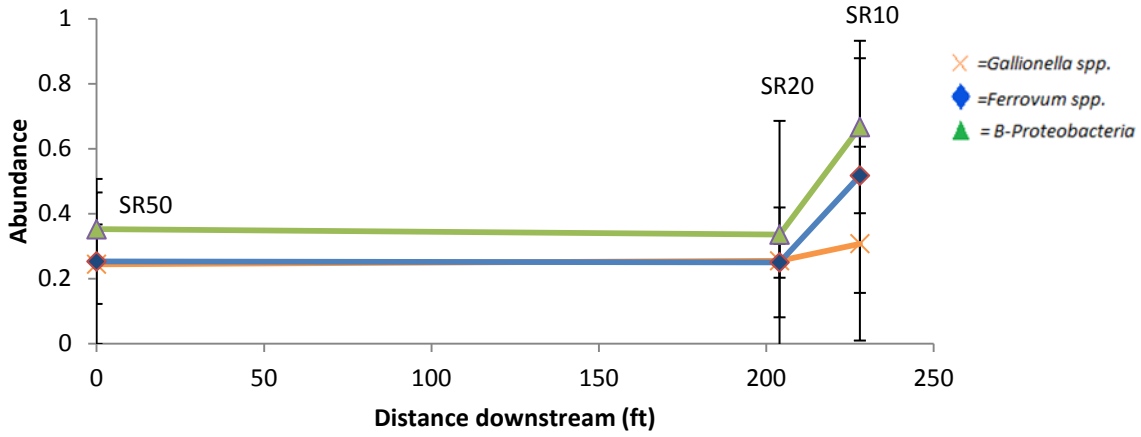

Figure 1. Sulphur Run stream profile of bacteria taxa abundance downstream. The orange x represents *Gallionella* spp. data points, the blue diamond represents *Ferrovum* spp. data points, and the green triangle represents β-proteobacteria data points. Sample ID numbers are indicated above the respective data points. Error bars were determined by calculating the standard deviation of individual taxa abundance counts for each picture taken per sample.

Table 5. Geochemistry and total FISH cell counts for each Sulphur Run sample location

Site ID	pH	[Fe2+]	Total Cells Counted
SR50	3.55	111.82	513
SR20	3.4	107.91	253
SR10	3.3	106.94	136

4.2 Windber Microbial distribution and abundance downstream

Acidithiobacillus, *Ferrovum*, and unknown β-proteobacteria are present in Windber. *Ferrovum* abundance exhibits a 10% variance range while *Acidithiobacillus* counts show almost no variance between sites (Figure 2). The most drastic change occurs within β-proteobacteria at site WB50 (52% β-proteobacteria) to site WB30 (35% β-proteobacteria). As in Sulphur Run FISH results, percent of taxa abundance observed never approaches 1.

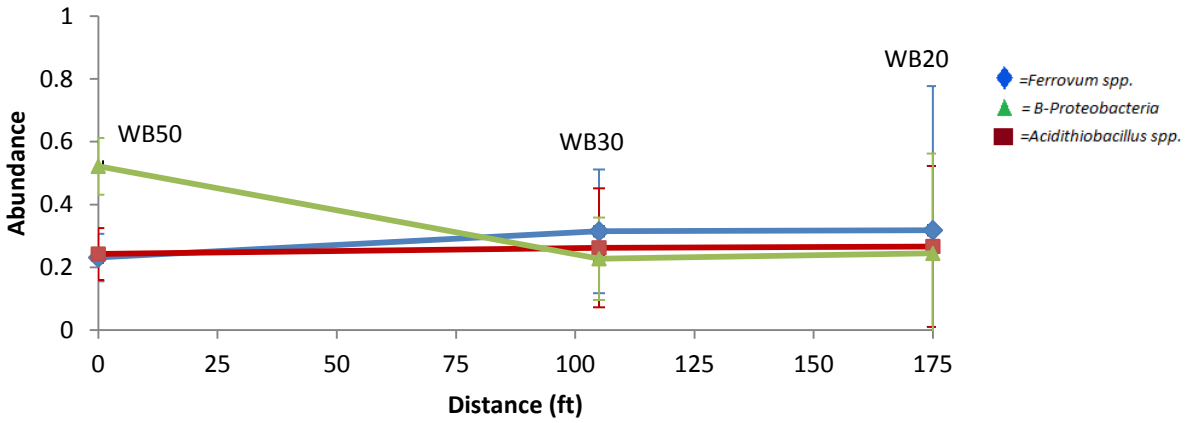

Figure 2. Windber stream profile of bacteria taxa abundance downstream. The red square represents *Acidithiobacillus spp*. data points, the blue diamond represents *Ferrovum spp*. data points, and the green triangle represents β-proteobacteria data points. Sample ID numbers are indicated above the respective data points. Error bars were determined by calculating the standard deviation of individual taxa abundance counts for each picture taken per sample.

Table 6. Geochemistry and total FISH cell counts for each Windber sample location

Site ID	pH	[Fe2+]	Total Cells Counted
WB50	2.9	105.96	4294
WB30	3.02	46.87632	1177
WB20	3.01	50.29439	190

4.3 Upper Red Eyes Microbial distribution and abundance downstream

FISH results from Upper Red Eyes samples show the presence of β-Proteobacteria, *Gallionella*, *Ferrovum*, and *Acidithiobacillus* (Figure 3). Each specific taxa displays a unique distribution throughout the stream while β-Proteobacteria hold a relatively steady abundance of around 70%-80% from the emergence to after 258 feet downstream (site UR80). After site UR80, the abundance of β-Proteobacteria decrease to just below 40% of the bacterial community. *Gallionella* make up just over 90% of the microbial community at site UR100 and decrease steadily downstream they are no longer present after site UR70. *Ferrovum* are 10% of the microbial abundance at the emergence to site UR84 52 feet downstream. At site UR83, however, *Ferrovum* abundance suddenly increases to 50% and decreases to a steady 10% abundance after site UR82. *Acidithiobacillus* are absent until 258 feet downstream at site UR70 where they make up 28% of the microbial community. Further downstream, *Acidithiobacillus* abundance decreases to 15%.

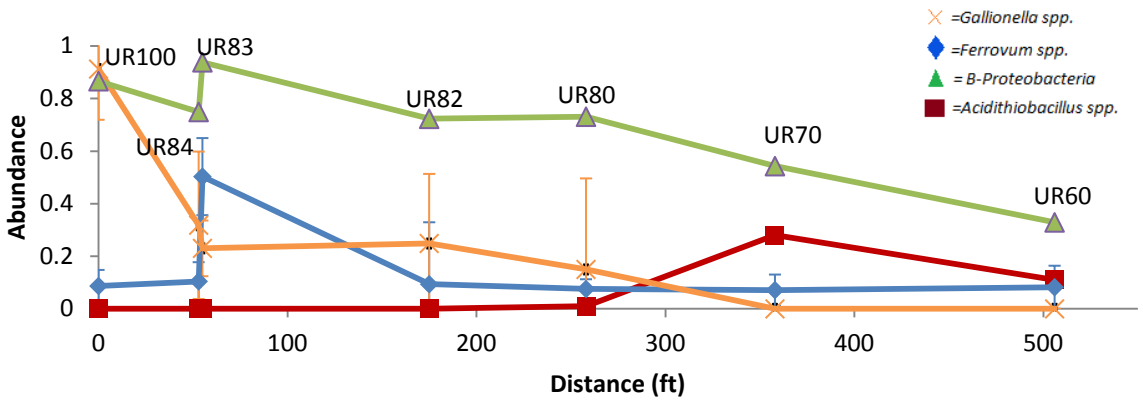

Figure 3. Upper Red Eyes stream profile of bacteria taxa abundance downstream. The red square represents *Acidithiobacillus spp.* data points, the blue diamond represents *Ferrovum spp.* data points, The orange X's represent *Gallionella spp.* and the green triangle represents β-proteobacteria data points. *Acidithiobacillus* and β-proteobacteria abundance values were provided by (Jones et al., In preparation). Sample ID numbers are indicated above the respective data points. Error bars were determined by calculating the standard deviation of individual taxa abundance counts for each picture taken per sample.

Table 7. Geochemistry and total FISH cell counts for each Upper Red Eyes sample location

Site ID	pH	$[Fe^{2+}]$	Total Cells Counted
UR100	4.01	388.6925	2046
UR84	3.53	375.5679	1361
UR83	3.255	204.947	1476
UR82	3.18	123.1701	511
UR80	3.125	153.4578	382
UR70	3.045	111.7893	127
UR60	2.945	79.84947	98

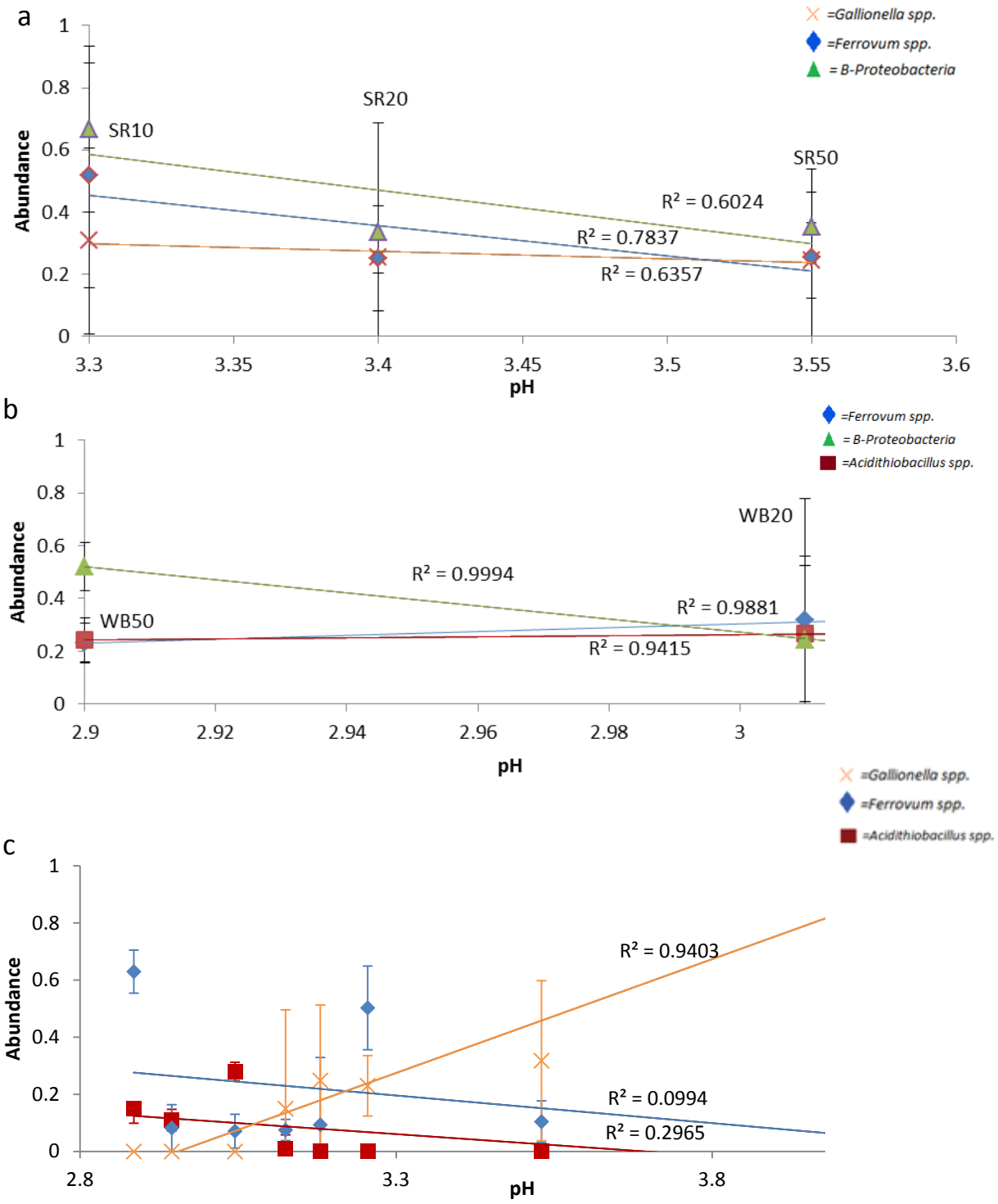

Figure 4. A. Sulphur Run, Windnber, and Upper Red Eyes relative bacteria abundance values respectively for *Gallionella* (orange X's), *Acidithiobacillus* (red squares), and *Ferrovum* (blue diamonds). R^2 values are indicated above the respective linear lines. Error bars were determined by calculating the standard deviation of individual taxa abundance counts for each picture taken per sample.

4.3 Abundance verse pH

Figure 4 shows relative bacterial abundance with respect to pH values from each AMD system. Sulphur Run (a) exhibits a moderate (R^2~ 0.6) correlation between bacterial relative abundance and pH for the three sites. Windber (b) shows a strong correlation ($R^2 > 0.9$) between all three sites. Upper Red Eyes(c) shows a very weak correlation ($R^2 < 0.4$) with *Ferrovum* and *Acidithiobacillus* relative abundance values and pH but a strong correlation with *Gallionella* relative abundance values. All other geochemical parameter abundance plots can be found in Appendix C.

4.4 Absolute abundance of bacteria cells counted

Figure 5 shows the absolute abundance for Upper Red Eyes shows an increase and decrease in each iron-oxidizing taxa at specific locations downstream from the emergence. The highest number of cells counted were from UR100 with over 1400 total bacterial cells. While the total number of bacteria cells counted decreased downstream, the dominant bacteria taxa varied between taxa.

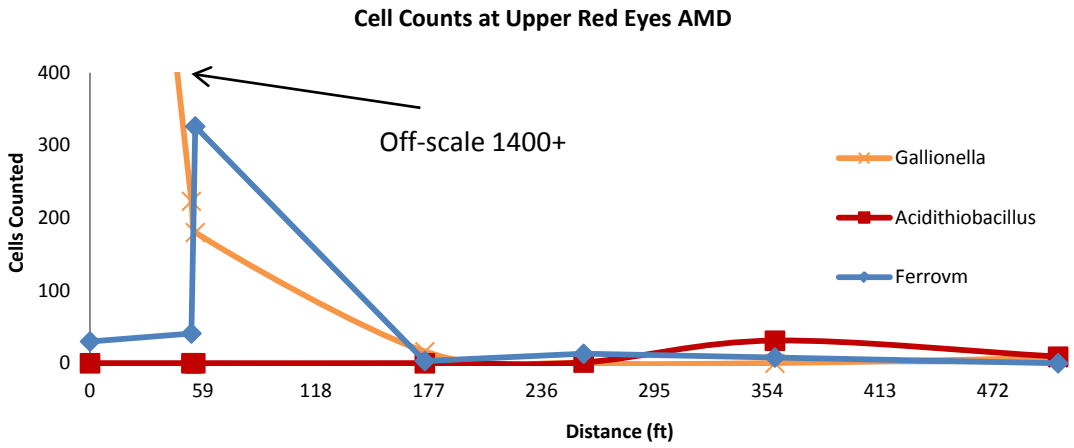

Figure 5. Absolute abundance of bacteria cells counted. Distance is shown on the x-axis and the number of cells counted is shown on the y-axis. The orange x's represent *Gallionella*, the red squares represent *Acidithiobacillus*, and the blue diamonds represent *Ferrovum.*

4.5 Niche comparison between Jones et al. (in review)

FISH results are mostly consistent with ecological niches from (Jones et al., In preparation) as shown by Figure 6. The most important difference to note is the increased *Gallionella* range of [Fe^{2+}] the results from our study create. While Jones et al. *Gallionella* niche clusters from 400 mg/L of [Fe^{2+}] to ~550 mg/L of [Fe^{2+}], our *Gallionella* results extends the proposed niche to [Fe^{2+}] =75mg/L. Unlike *Gallionella* results, *Ferrovum* and *Acidithiobacillus* abundance and distribution strongly agree with Jones *et al*.'s proposed ecological niches.

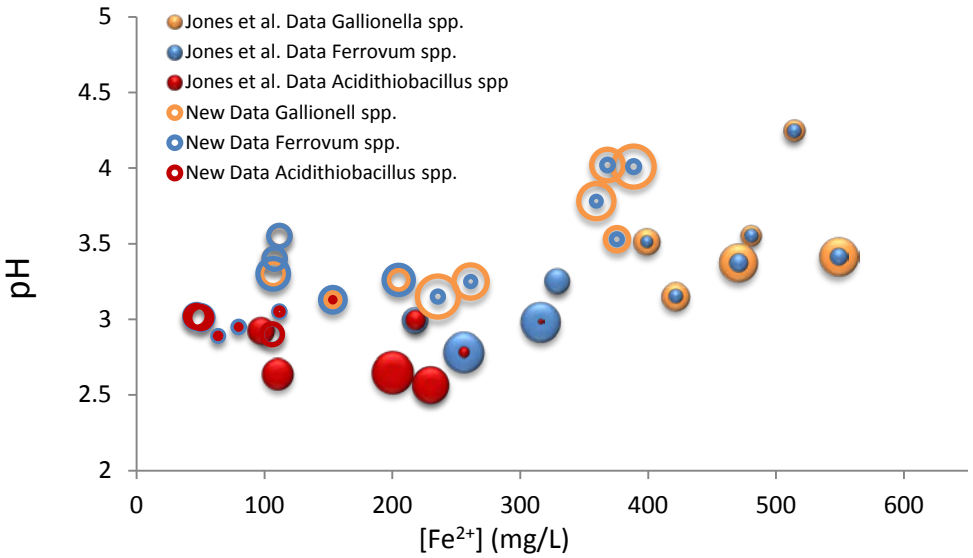

Figure 6. Comparison of AMD bacteria taxa abundance and pH/ [Fe^{2+}] distribution between this study and (Jones et al., In preparation). Results from this study are indicated by unfilled abundance circles and results from Jones et al. are indicated by filled abundance circles. The size of the circle represents the abundance and the colors represent the different taxa. The model was created in Excel.

4.6 Ecological niche models associated with AMD bacteria

The combined models from our results and (Jones et al., In preparation) AMD results (Figure 7) create three main 'zones'. The *Gallionella* zone (indicated in red) ranges from [Fe^{2+}] >200 mg/L <600 mg/L and pH >3. *Acidithiobacillus* clusters within a zone of [Fe^{2+}] <270 mg/L and pH >2 < 3.5. *Ferrovum* appear to have a comparatively larger ecological niche and overlap with *Gallionella* a considerable amount, however the optimal parameters, as shown by the large relative abundance, are pH 2.5 -3 and [Fe^{2+}] between 200mg/L - 350 mg/L.

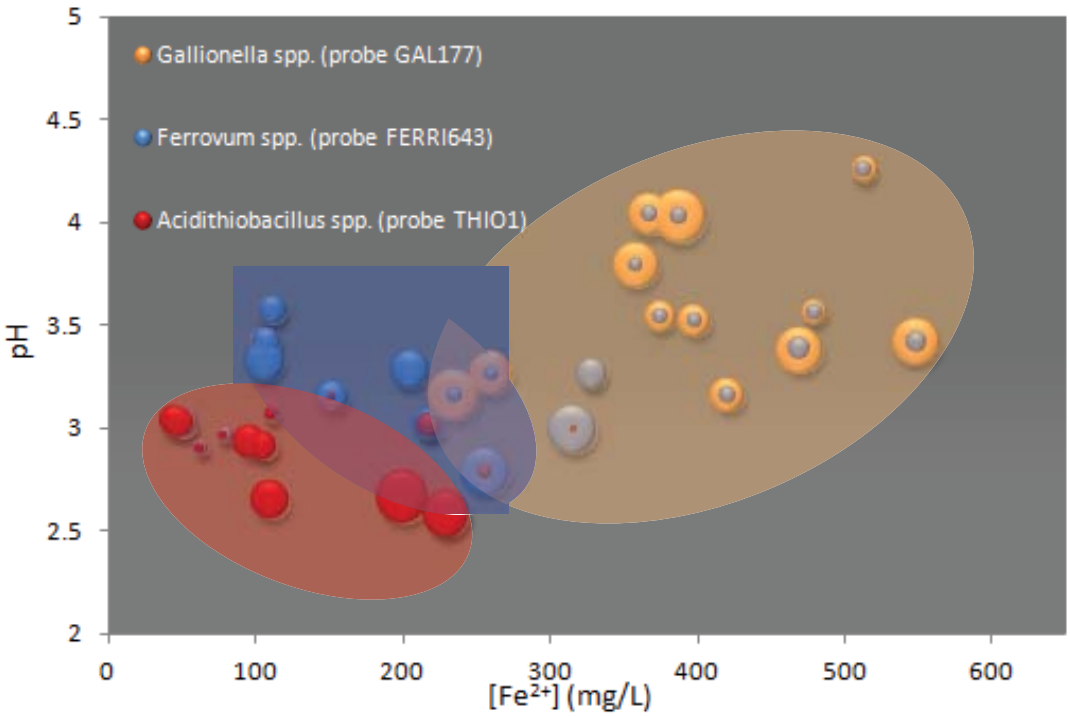

Figure 7. Proposed AMD ecological niche model. The model consists of results from this study and (Jones et al., In preparation). The size of the circle represents the abundance and the colors represent the different taxa. The model was created in Excel.

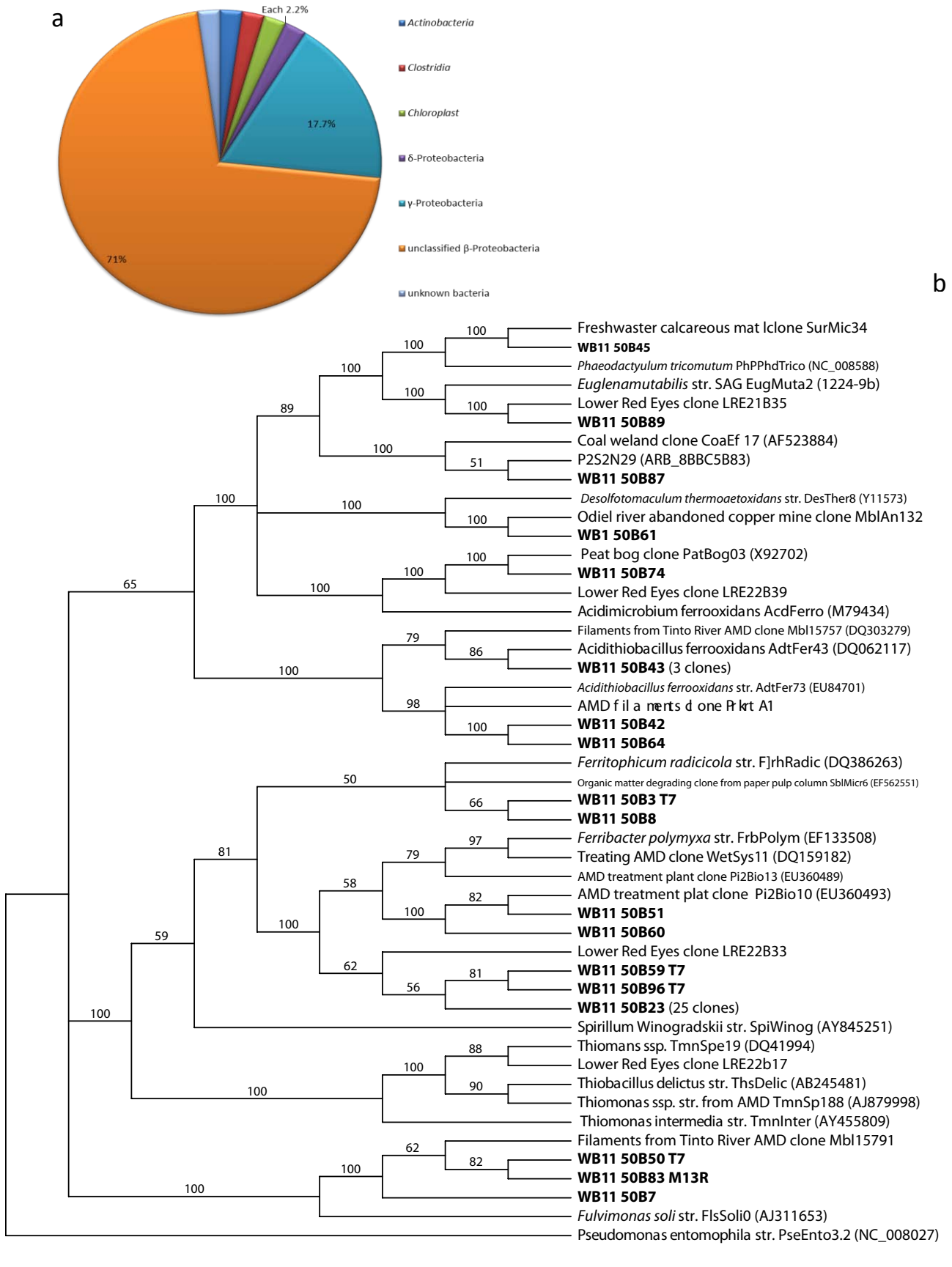

Figure 8. (a) Class-level distribution of 16S rRNA sequences obtained from the emergent sediments of WB50. (b) Maximum-parsimony tree showing the phylogenetic relationship of the clones obtained from these sediments.Bootstrap values for nodes greater than 50% support, determined with 1,000 replicates, are displayed as percentages. GenBank accession numbers are in parentheses.

4.7 Taxonomic affiliation and phylogenetic relationship of sequenced clones

Results from DNA extraction and clone sequencing from site WB50 reveal 71% of the bacteria are classified under unknown β-proteobacteria and 17.7% are characterized as γ-proteobacteria (Figure 8). The remaining clones classify under *Actinobacteria, Clostridia, Chloroplast*, and δ-proteobacteria in equal abundance. Figure 8 displays the evolutionary relationship of the WB50 sequences and archived sequences. Distances reveal the majority of WB50 sequences are β-proteobacteria as and are closely related to bacteria within the class *Ferrovum*. The characterized γ-proteobacteria are closely related to *Acidimicrobium ferrooxidans* and *Acidthiobacillus ferrooxidans*. Three of the WB50 sequences are closely related to sequences from the class *Xanthomonadales.* Sequences WB11 50B45 and WB11 50B89 are closely related to a *Euglenamutabilis* str. All of the WB50 sequences are closely related to Lower Red Eyes and other AMD sequences.

5.0 Discussion

5.1 Niche model analysis

Our results suggest a niche model analysis is the most accurate way to describe the ecological distribution of iron-oxidizing bacterial communities within AMD. When extrapolated onto (Jones et al., In preparation) pH/ [Fe^{2+}] niche model, correlations between the geochemical parameters and taxa distribution and abundance are apparent. Adversely, FISH results generally exhibit a weak correlation with pH independently. Similar correlations exist between bacteria abundance and other geochemical values i.e. [Fe^{2+}], temperature, etc. (refer to Appendix B). This suggests the relationships and interdependence between microbial communities and environmental parameters are more complex than simply a correlation between a single geochemical factor and the residing biology. Our findings are consistent with earlier research exploring the interaction of geochemistry and microbiology (Gonzalez-Toril et al., 2011; He et al., 2007; Lear et al., 2009; Macalady et al., 2008). For instance, Macalady et al. (2008) found sulfidic cave-dwelling biofilms reside in environmental niches established by dissolved oxygen and total sulfide concentrations. The accruing evidence indicates the necessity of ecological niches to determine and describe the bacterial abundance within any environment.

The geochemical determination of bacterial distribution hypothesis is further supported by the comparison between relative and absolute abundance data. Absolute abundances exhibit similar trends as relative abundances indicating interdependence between iron-oxidizing bacteria species. This could suggest that the different iron-oxidizing bacteria are competing with one another and each species outcompetes the other within specific geochemical conditions.

Environmental niche models may help to describe niche-driven evolutionary divergence. Oakley et al. (2010) discovered a strong relationship between genetic distance and both

environmental distance and geographic distance. Their results are evidence for ecological niche partitioning and evolutionary divergence of locally adapted populations and clearly observable biogeographic patterns (Oakley et al., 2010). This supports the hypothesis that environmental niches (as opposed to single environmental parameters) are the fundamental cause and method for evolution and species divergence and subsequent species distribution.

4.3 Comparison of abundance and distribution between AMD systems

Sulphur Run and Windber are AMD systems with consistent geochemical values throughout the stream and the generally constant relative abundance of *Ferrovum* and *Gallionella* reflect this characteristic. It is also interesting to note that *Gallionella* and *Ferrovum* abundances are equal within and between each stream. Upper Red Eyes results are very different in that the geochemistry changes drastically from the emergence to downstream. The Upper Red Eyes stream abundance profile (Figure 3) reflects the geochemical changes. *Gallionella*, *Ferrovum*, and *Acidithiobacillus* all have sites of ideal geochemical conditions. It is important to note that in all of the AMD systems, regardless of geochemical conditions, cell density is highest near the emergence and decreases downstream. This characteristic may be due to a decrease in nutrients downstream from the emergence from phosphate sorption to iron oxides (Simmons, 2010).

5.3 Issues in FISH results

Although using the probe Bet42a is reasonable, some ambivalence exists within the FISH results. For instance, sites WB30 and WB20 show counts that are lower than *Ferrovum* counts. This is intuitively impossible because *Ferrovum* is a known β-proteobacteria thus, the total Beta counts should account for the *Ferrovum* abundance. This disconnect may be due to 1) inadequacies in the Bet42a probe and/or 2) high error associated with abundance due to insufficient cell counts. To improve FISH results and total abundance, Bet42a should be

improved or only used as a preliminary probe. Similarly, to reduce uncertainty in any of the abundance results, additional FISH counts should be done on most of the samples from each of the three AMD. Sulphur Run total cell counts never exceed 1,000. Such low cell counts create very large error bars. Similarly, observations from Upper Red Eyes indicate the short distance with which geochemistry as well as microbial structure can change in an AMD system. Windber and Sulphur Run samples were only collected from three different locations, each a considerable distance from each other. It is possible both the geochemistry and microbial configuration change significantly between the sampled locations.

5.4 Bacteria characterization from clone sequencing

Results from the environmental DNA sequencing agree with previous studies showing the presence of *Ferrovum* and *Acidithiobacillus* (Gonzalez-Toril et al., 2011; He et al., 2007; Heinzel et al., 2009; Lear et al., 2009). The presence of *Xanthomonadales* has not been as well discussed and demands further investigation. *Lysobacter* is clade within Xanthomonadales and specific sequences within *Lysobacter* have been obtained from extreme environments such as hydrothermal vents from an iron-oxidizing microaerophilic lithotroph (Bae et al., 2005). The potential presence of this iron-oxidizing bacteria is cause for further examination.

4.4 Future Investigations

An understanding of the microbial composition response to changing conditions is needed to fully understand the interplay between biology and the environment. The seasonal variations in the geochemistry of AMD have been well documented (Butler et al., 2008; Elberling, 2001; Herr and Gray, 1996; Sarmiento et al., 2009). Sarmiento et al. (2009) found that the M/Fe ratio (M = metals other than Fe) decreases during the summer in highly contaminated streams affected by AMD. A regularly sampled AMD over a long time span may help to reveal the most influential geochemical parameters determining the microbial community structure.

Documenting the responses of each AMD microbial taxa with changing geochemical conditions could unveil key environmental conditions that, combined, create various microbial niches. Such research has further application. Seasonal change within AMD and the resulting microbial structure changes may prohibit applied bioremediation within an AMD system. Exploring the rates and extents of bacteria responses may result in durable and stable bioremediation methods.

6.0 Conclusion

The results from the present study strengthened the notion that a pH/ [Fe^{2+}] niche model best describes the community structure of iron-oxidizing bacteria and indicated that species affiliated with *Gallionella*, *Ferrovum*, and *Acidithiobacillus* cluster within separate pH/[Fe^{2+}] ranges. A correlation between this niche model and the bacterial relative abundance stream profile was made and further correlated with the absolute bacterial cell counts. Similar trends within each analysis supports the hypothesis that the geochemistry of an AMD system determines the iron-oxidizing bacteria abundance and strongly suggests an interdependence and competition between the bacteria species. Results from this study render the expanded pH/[Fe^{2+}] niche model accurate and available for bioremediation application. This model may allow environmental engineers to predict the iron-oxidizing bacterial community composition and structure without microbiological analysis techniques.

7.0 Acknowledgments

This work was supported by the National Science Foundation under grant no. CHE-0431328, by the Pennsylvania Department of Environmental Protection, Bureau of Abandoned Mine Reclamation, and by the Undergraduate Geoscience Department at Penn State University for a grant I used to sequence the samples from Windber. I thank my advisor, Dr. Jennifer Macalady for her advice and guidance. I thank Irene Schaperdoth, Dan Jones, and Christy Miller for their continuous help and support. Finally, I thank Dr. William Burgos and Lance Larson for inviting me to the AMD sites and for allowing me to use their geochemical measurements for each stream.

8.0 References

Altschul, S.F., Gish, W., Miller, W., Myers, E.W., and Lipman, D.J., 1990, BASIC LOCAL ALIGNMENT SEARCH TOOL: Journal of Molecular Biology, v. 215, p. 403-410.

Bae, H.S., Im, W.T., and Lee, S.T., 2005, Lysobacter concretionis sp. nov., isolated from anaerobic granules in an upflow anaerobic sludge blanket reactor: International Journal of Systematic and Evolutionary Microbiology, v. 55, p. 1155-1161.

Baker, B.J., and Banfield, J.F., 2003, Microbial communities in acid mine drainage: Fems Microbiology Ecology, v. 44, p. 139-152.

Brown, J.F., Jones, D.S., Mills, D.B., Macalady, J.L., and Burgos, W.D., 2011, Application of a Depositional Facies Model to an Acid Mine Drainage Site: Applied and Environmental Microbiology, v. 77, p. 545-554.

Butler, B.A., Ranville, J.F., and Ross, P.E., 2008, Observed and modeled seasonal trends in dissolved and particulate Cu, Fe, Mn, and Zn in a mining-impacted stream: Water Research, v. 42, p. 3135-3145.

Cole, J.R., Chai, B., Marsh, T.L., Farris, R.J., Wang, Q., Kulam, S.A., Chandra, S., McGarrell, D.M., Schmidt, T.M., Garrity, G.M., and Tiedje, J.M., 2003, The Ribosomal Database Project (RDP-II): previewing a new autoaligner that allows regular updates and the new prokaryotic taxonomy: Nucleic Acids Research, v. 31, p. 442-443.

de Wit, R., and Bouvier, T., 2006, 'Everything is everywhere, but, the environment selects'; what did Baas Becking and Beijerinck really say?: Environmental Microbiology, v. 8, p. 755-758.

DeSantis, T.Z., Hugenholtz, P., Larsen, N., Rojas, M., Brodie, E.L., Keller, K., Huber, T., Dalevi, D., Hu, P., and Andersen, G.L., 2006, Greengenes, a chimera-checked 16S rRNA gene database and workbench compatible with ARB: Applied and Environmental Microbiology, v. 72, p. 5069-5072.

Druschel, G.K., Baker, B.J., Gihring, T.M., and Banfield, J.F., 2004, Acid mine drainage biogeochemistry at Iron Mountain, California: Geochemical Transactions, v. 5, p. 13-32.

Dsa, J.V., Johnson, K.S., Lopez, D., Kanuckel, C., and Tumlinson, J., 2008, Residual toxicity of acid mine drainage-contaminated sediment to stream macroinvertebrates: Relative contribution of acidity vs. metals: Water Air and Soil Pollution, v. 194, p. 185-197.

Elberling, B., 2001, Environmental controls of the seasonal variation in oxygen uptake in sulfidic tailings deposited in a permafrost-affected area: Water Resources Research, v. 37, p. 99-107.

Engineers, U.S.A.C.o., 1969.

Gerhardt, A., de Bisthoven, L.J., Guhr, K., Soares, A., and Pereira, M.J., 2008, Phytoassessment of acid mine drainage: Lemna gibba bioassay and diatom community structure: Ecotoxicology, v. 17, p. 47-58.

Gonzalez-Toril, E., Aguilera, A., Souza-Egipsy, V., Pamo, E.L., Espana, J.S., and Amils, R., 2011, Geomicrobiology of La Zarza-Perrunal Acid Mine Effluent (Iberian Pyritic Belt, Spain): Applied and Environmental Microbiology, v. 77, p. 2685-2694.

He, Z.G., Xiao, S.M., Xie, X.H., Zhong, H., Hu, Y.H., Li, Q.H., Gao, F.L., Li, G.Y., Liu, J.S., and Qiu, G.Z., 2007, Molecular diversity of microbial community in acid mine drainages of Yunfu sulfide mine: Extremophiles, v. 11, p. 305-314.

Heinzel, E., Janneck, E., Glombitza, F., Schlomann, M., and Seifert, J., 2009, Population Dynamics of Iron-Oxidizing Communities in Pilot Plants for the Treatment of Acid Mine Waters: Environmental Science & Technology, v. 43, p. 6138-6144.

Herr, C., and Gray, N.F., 1996, Seasonal variation of metal contamination of riverine sediments below a copper and sulphur mine in South-East Ireland: Water Science and Technology, v. 33, p. 255-261.

Huber, T., Faulkner, G., and Hugenholtz, P., 2004, Bellerophon: a program to detect chimeric sequences in multiple sequence alignments: Bioinformatics, v. 20, p. 2317-2319.

Jones, D., C. Kolesar, L. Larson, J. Brown, D. Mills, W. Burgos, and Macalady, J., In preparation, Ecological niches of Fe-oxidizing acidophiles in a coal mine discharge.

Lear, G., Niyogi, D., Harding, J., Dong, Y.M., and Lewis, G., 2009, Biofilm Bacterial Community Structure in Streams Affected by Acid Mine Drainage: Applied and Environmental Microbiology, v. 75, p. 3455-3460.

Ludwig, W., Strunk, O., Westram, R., Richter, L., Meier, H., Yadhukumar, Buchner, A., Lai, T., Steppi, S., Jobb, G., Forster, W., Brettske, I., Gerber, S., Ginhart, A.W., Gross, O., Grumann, S., Hermann, S., Jost, R., Konig, A., Liss, T., Lussmann, R., May, M., Nonhoff, B., Reichel, B., Strehlow, R., Stamatakis, A., Stuckmann, N., Vilbig, A., Lenke, M., Ludwig, T., Bode, A., and Schleifer, K.H., 2004, ARB: a software environment for sequence data: Nucleic Acids Research, v. 32, p. 1363-1371.

Macalady, J.L., Dattagupta, S., Schaperdoth, I., Jones, D.S., Druschel, G.K., and Eastman, D., 2008, Niche differentiation among sulfur-oxidizing bacterial populations in cave waters: Isme Journal, v. 2, p. 590-601.

McKnight, D.M., and Feder, G.L., 1984, THE ECOLOGICAL EFFECT OF ACID CONDITIONS AND PRECIPITATION OF HYDROUS METAL-OXIDES IN A ROCKY-MOUNTAIN STREAM: Hydrobiologia, v. 119, p. 129-138.

Meyer, K.M., and Leveau, J.H.J., 2012, Microbiology of the phyllosphere: a playground for testing ecological concepts: Oecologia, v. 168, p. 621-629.

Mohapatra, B.R., Gould, W.D., Dinardo, O., and Koren, D.W., 2011, Tracking the prokaryotic diversity in acid mine drainage-contaminated environments: A review of molecular methods: Minerals Engineering, v. 24, p. 709-718.

Nancucheo, I., and Johnson, D.B., 2011, Significance of Microbial Communities and Interactions in Safeguarding Reactive Mine Tailings by Ecological Engineering: Applied and Environmental Microbiology, v. 77, p. 8201-8208.

Oakley, B.B., Carbonero, F., van der Gast, C.J., Hawkins, R.J., and Purdy, K.J., 2010, Evolutionary divergence and biogeography of sympatric niche-differentiated bacterial populations: Isme Journal, v. 4, p. 488-497.

Sarmiento, A.M., Nieto, J.M., Casiot, C., Elbaz-Poulichet, F., and Egal, M., 2009, Inorganic arsenic speciation at river basin scales: The Tinto and Odiel Rivers in the Iberian Pyrite Belt, SW Spain: Environmental Pollution, v. 157, p. 1202-1209.

Sheoran, A.S., and Sheoran, V., 2006, Heavy metal removal mechanism of acid mine drainage in wetlands: A critical review: Minerals Engineering, v. 19, p. 105-116.

Simmons, J.A., 2010, Phosphorus Removal by Sediment in Streams Contaminated with Acid Mine Drainage: Water Air and Soil Pollution, v. 209, p. 123-132.

Swofford, D., 2000, PAUP* Phylogenetic Analysis Using Parsimony and Other Methods (Software): Sunderland, MA., Sinauer Associates.

Templeton, A.S., 2011, Geomicrobiology of iron in Extreme Environments: Elements, v. 7, p. 95-100.

Weber, K.P., Werker, A., Gehder, M., Senger, T., and Legge, R.L., 2010, Influence of the Microbial Community in the Treatment of Acidic Iron-Rich Water in Aerobic Wetland Mesocosms: Bioremediation Journal, v. 14, p. 28-37.

Appendix A

Locations of AMD studied

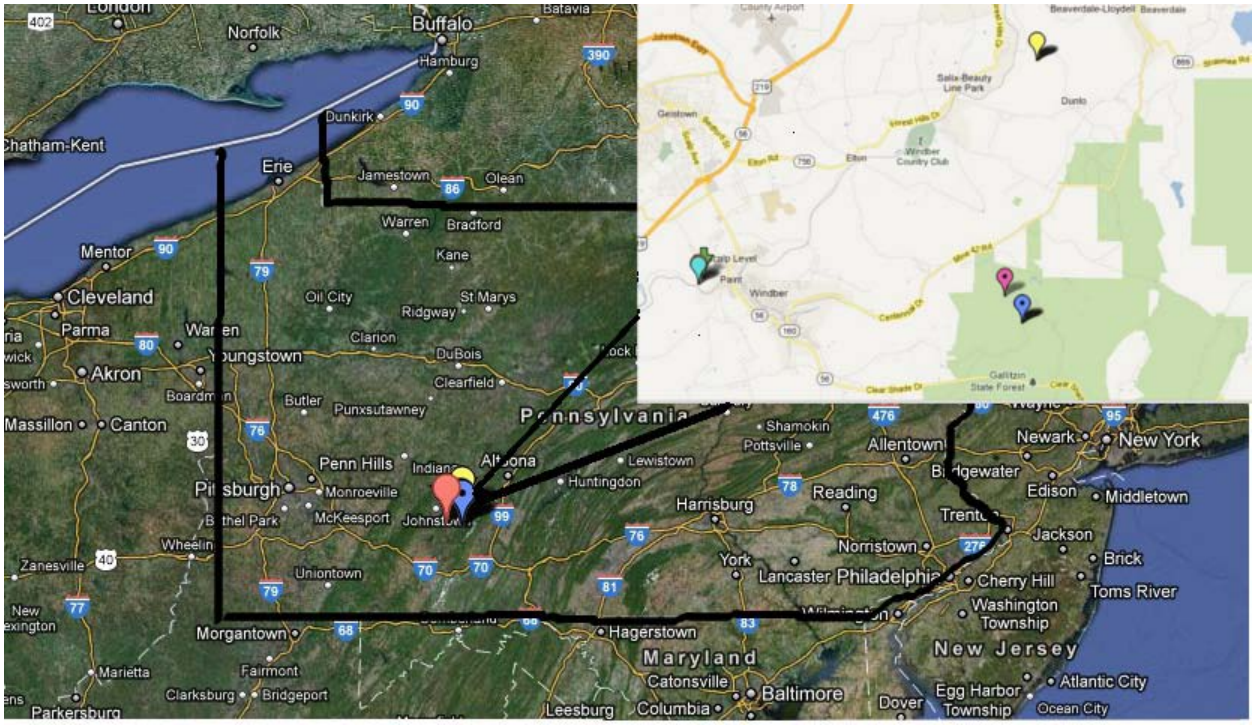

Map view of AMD locations examined in this study. Yellow pinpoint represents Sulphur Run (40°18’25.91” N; 78°44’5.06”W), light blue pinpoint represents Windber (40°14’43.72” N; 78°51’33.18”W), dark blue pinpoint with black center represents Lower Red Eyes (40°14’24.90” N; 78°44’48.92”W)and purple pinpoint with black center represents Upper Red Eyes (40°14’27.07” N; 78°44’25.42”W) from Jones et al. (*in preparation*).

Geochemistry of AMD studied

Sulphur Run Geochemistry

Site ID	Distance from emergence (ft)	pH	Total Fe (mg/L)	[Fe2+] (mg/L)	Conductivity (uS/cm)	Temperature (°C)	ORP (mV)
SR50	0	3.55	114.5484	111.8196	895	10.55	281
SR20	204	3.4	111.6238	107.9132	913	11.15	359
SR10	228	3.3	110.1614	106.9366	922.5	11.45	348

Windber Geochemistry

Site ID	Distance from emergence (ft)	pH	Total Fe (mg/L)	[Fe2+] (mg/L)	Conductivity (uS/cm)	Temperature (°C)	ORP (mV)
WB50	0	2.9	108.21	105.96	2.04	13.4	333.33
WB30	105	3.02	81.88	46.87	2.26	19.3	502.5
WB20	175	3.01	80.91	50.29	2.2	19.7	460

Upper Red Eyes Geochemistry

Site ID	Distance from emergence (ft)	pH	Total Fe (mg/L)	[Fe2+] (mg/L)	Conductivity (uS/cm)	Temperature (°C)	ORP (mV)
UR100	0	4.01	385.285164	388.6925	2.69	9.45	306
UR84	53	3.53	373.369128	375.5679	2.05	10.40	363
UR83	55	3.255	222.432672	204.947	1.7	12.7	400
UR82	175	3.18	131.076396	123.1701	1.555	13.9	394
UR80	258	3.125	163.845495	153.4578	2.12	17	398.5
UR70	358	3.045	142.992432	111.7893	2.07	17.95	437
UR60	506	2.945	119.701998	79.84947	2.46	20.1	458

Appendix B: FISH pics

FISH pictures taken from WB50 with (a) DAPI, (b) Eubmix FITC and DAPI, (c) Ferri643, and (d) all three probes.

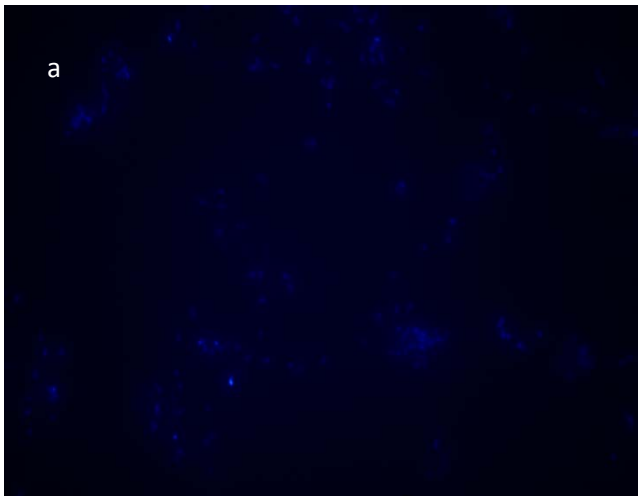

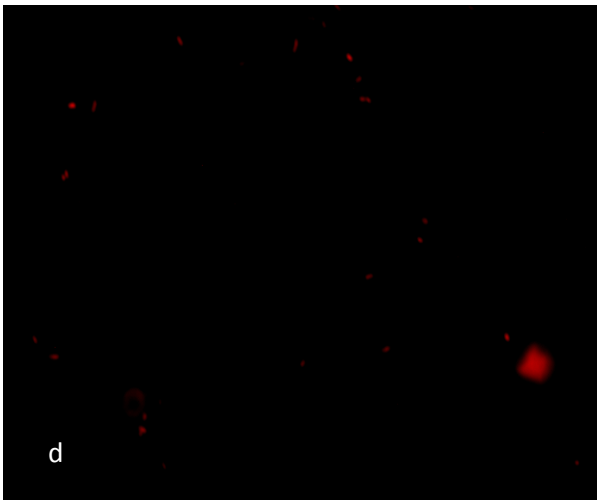

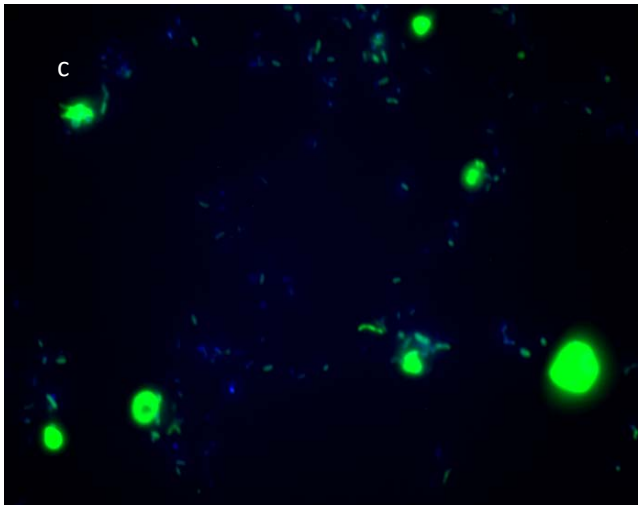

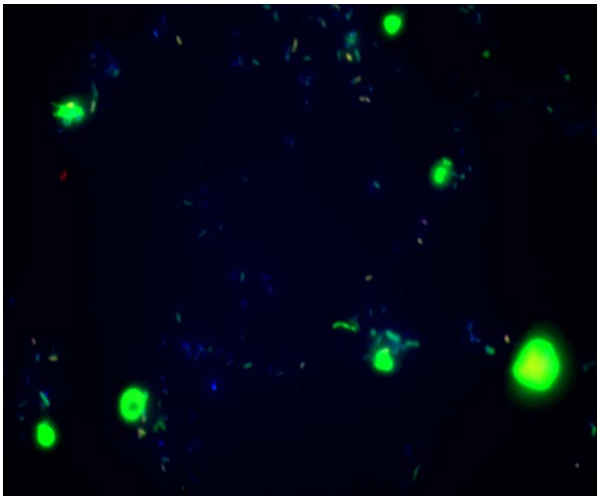

Appendix C

Sulphur Run

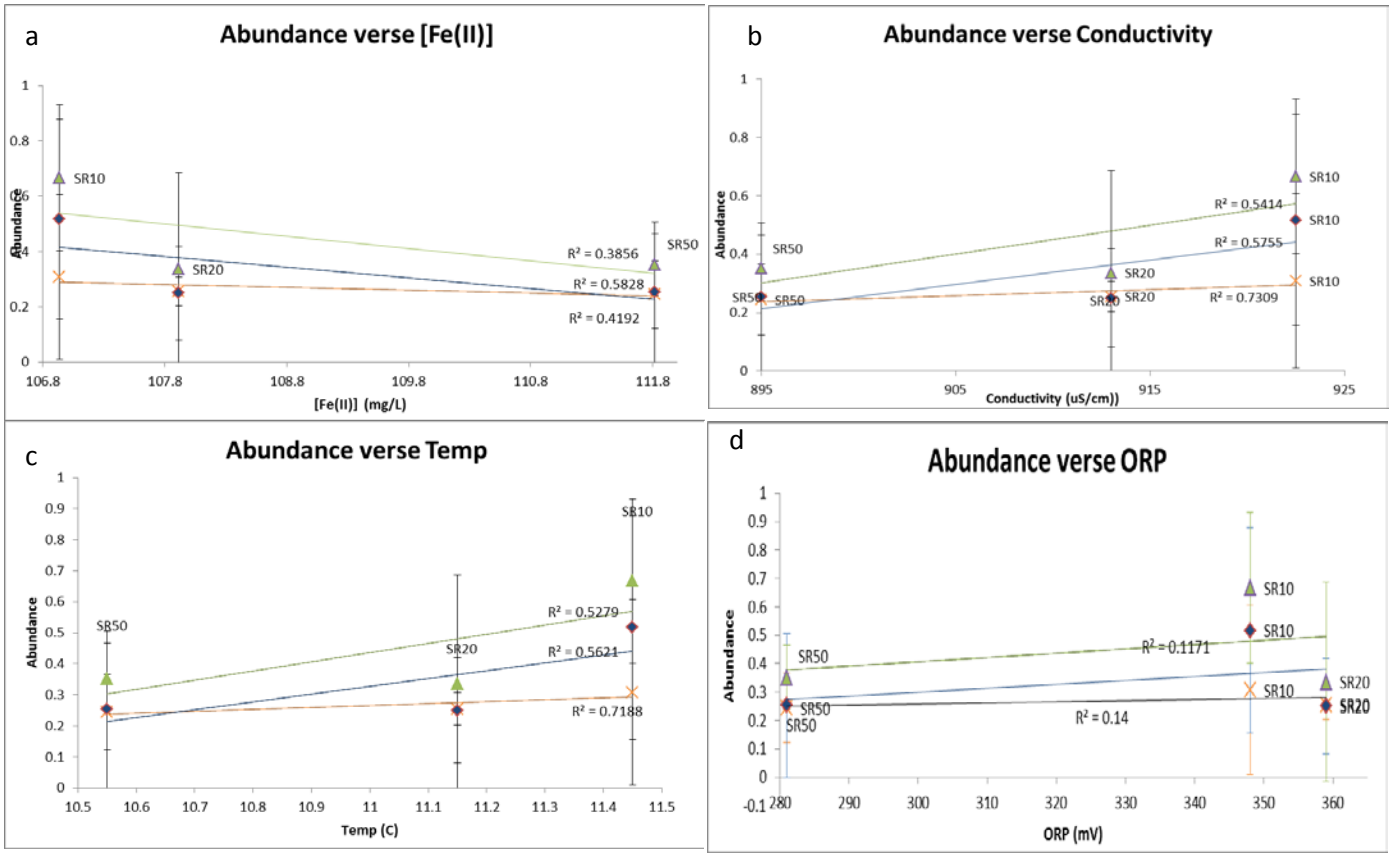

Sulphur Run abundance values verses, [Fe2+] (a), conductivity (b), temperature (c), and ORP (d). The orange x represents *Gallionella* spp. data points, the blue diamond represents *Ferrovum* spp. data points, and the green triangle represents β-proteobacteria data points. Sample ID numbers are indicated above the respective data points. Error bars were determined by calculating the standard deviation of individual taxa abundance counts for each picture taken per sample.

Windber

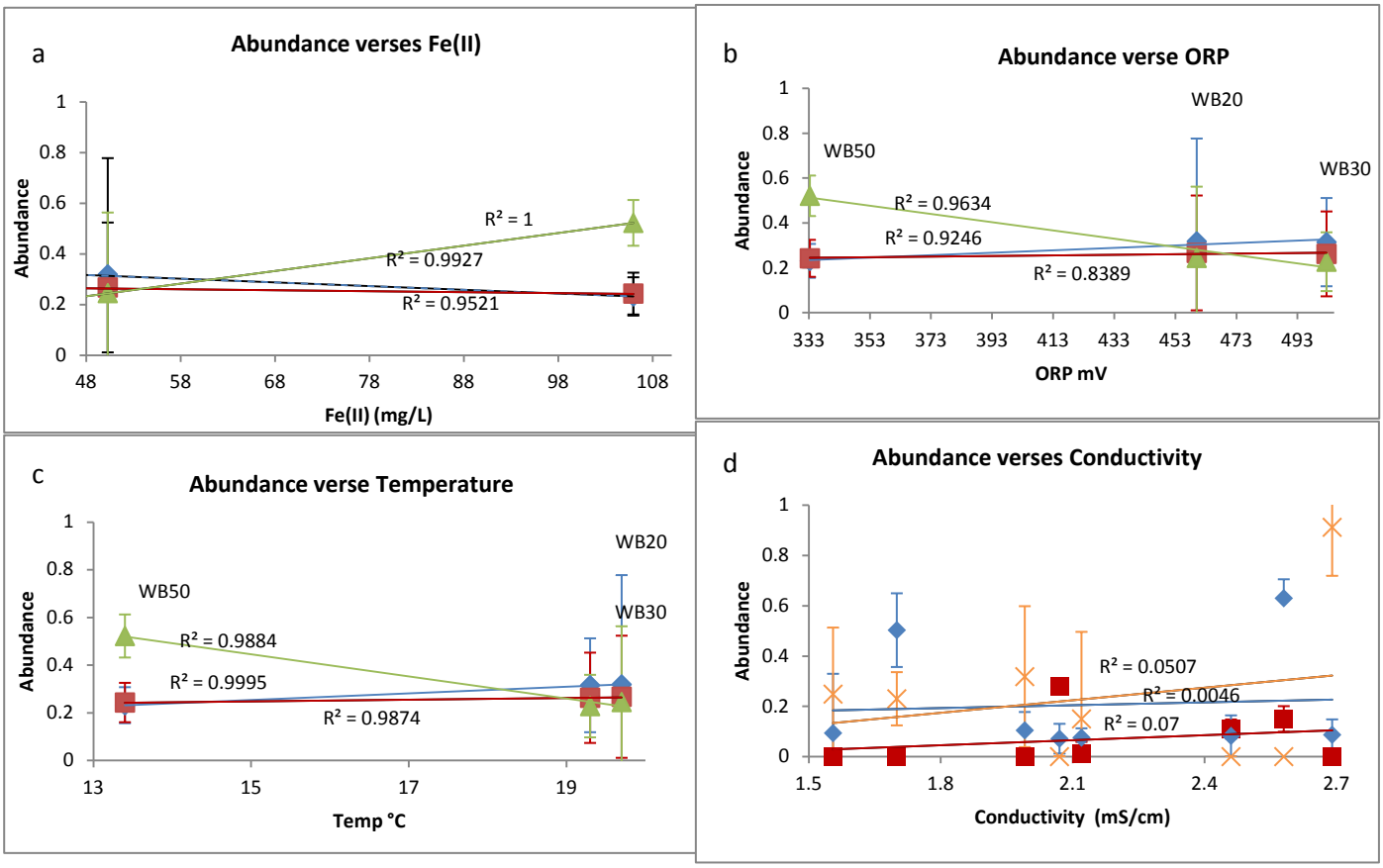

Windber abundance values verses, [Fe2+] (a), conductivity (b), temperature (c), and ORP (d). Red squares represent *Acidithiobacillus* spp. data points, blue diamonds represent *Ferrovum* spp. data points, and green triangles represent β-proteobacteria data points. Sample ID numbers are indicated above the respective data points. Error bars were determined by calculating the standard deviation of individual taxa abundance counts for each picture taken per sample.

Upper Red Eyes

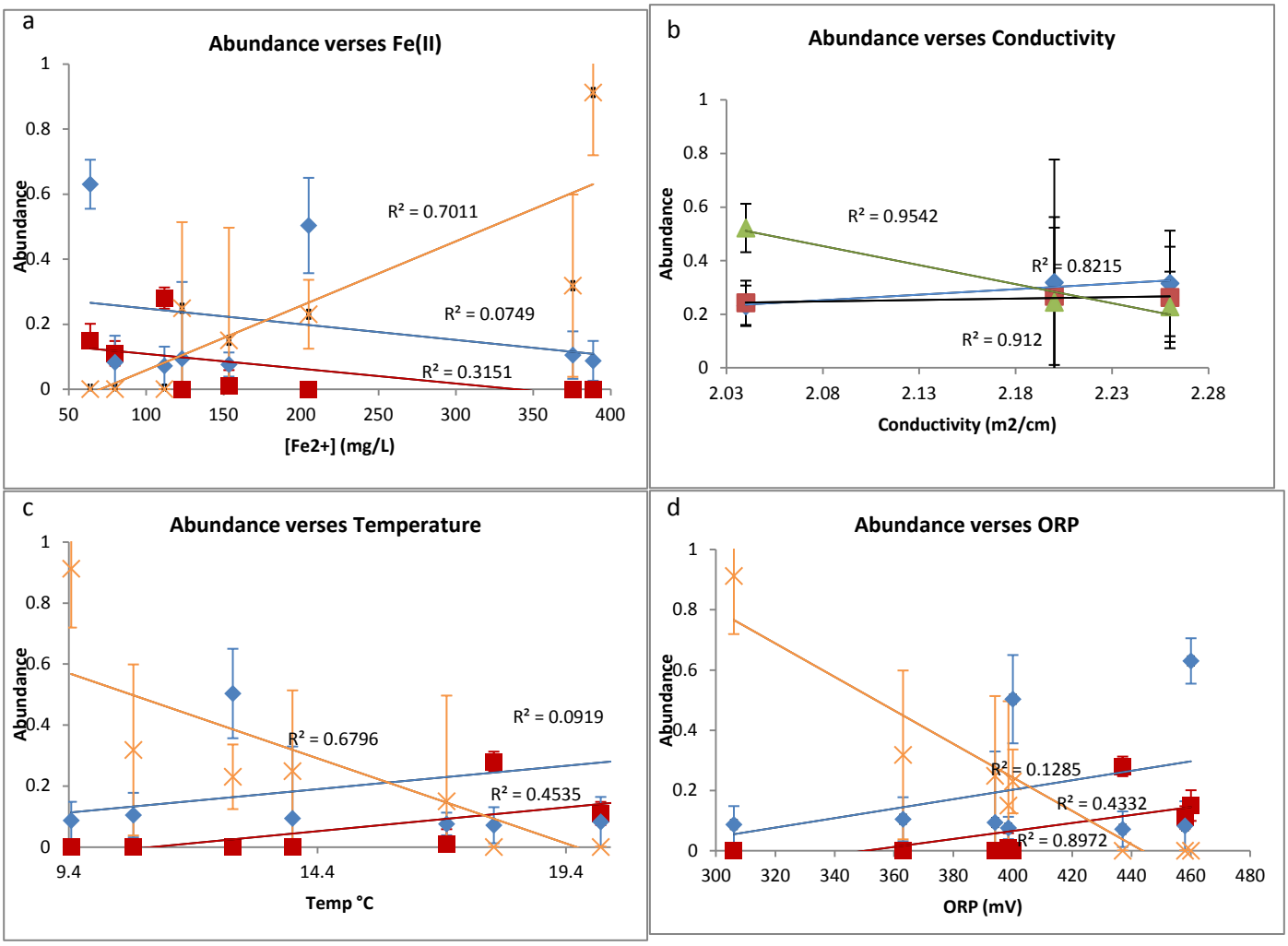

Upper Red Eyes abundance values verses, [Fe2+] (a), conductivity (b), temperature (c), and ORP (d). Red squares represent *Acidithiobacillus* spp. data points, blue diamonds represent *Ferrovum* spp. data points, orange x's represent Gallionella spp. Abundance values, and green triangles represent β-proteobacteria data points. Sample ID numbers are indicated above the respective data points. Error bars were determined by calculating the standard deviation of individual taxa abundance counts